Theoretical electron-impact-ionization cross section for Fe^{11+} forming Fe^{12+}

Duck-Hee Kwon[1] and Daniel Wolf Savin[2]

[1]*Nuclear Data Center, Korea Atomic Energy Research Institute, Daejeon 305-353, Republic of Korea*

[2]*Columbia Astrophysics Laboratory, Columbia University, New York, New York 10027, USA*

(Received 14 June 2012; published 1 August 2012)

We have calculated cross sections for electron impact ionization (EII) of P-like Fe^{11+} forming Si-like Fe^{12+}. We have used the flexible atomic code (FAC) and a distorted-wave (DW) approximation. Particular attention has been paid to the ionization through the $3l \rightarrow nl'$ and $2l \rightarrow nl'$ excitation autoionization (EA) channels. We compare our results to previously published FAC DW results and recent experimental results. We find that the previous discrepancy between theory and experiment at the EII threshold can be accounted for by the $3l \rightarrow nl'$ EA channels which were not included in the earlier calculations. At higher energies the discrepancy previously seen between theory and experiment for the magnitude of the $2l \rightarrow nl'$ ($n \geqslant 4$) EA remains, though the difference has been reduced by our newer results. The resulting Maxwellian rate coefficient derived from our calculations lies within 11% of the experimentally derived rate coefficient in the temperature range where Fe^{11+} forms in collisional ionization equilibrium.

DOI: 10.1103/PhysRevA.86.022701 PACS number(s): 34.80.Dp

I. INTRODUCTION

Our understanding of laboratory and astrophysical plasmas rests, in part, on knowledge of the underlying charge state distribution (CSD) of the gas. Accurate CSD data are needed to determine and model physical properties such as the thermal structure and line emission of these plasmas [1–3]. Our work here is relevant to collisionally ionized plasmas where the CSD is determined by the balance between electron impact ionization (EII) and electron-ion recombination [4].

Taking into account the EII data needs of the various scientific and engineering communities, data are required for essentially all charge states of all elements. However, of particular importance are reliable data for Fe ions. For example, tokamak and other plasma devices are typically constructed using stainless steel containment vessels, making Fe sputtered from the walls a common contaminant in the plasma devices [5]. In astrophysics, Fe is cosmically abundant and is seen in collisionally ionized sources such as the Sun [6], stars [7], galaxies [8], clusters of galaxies [9], and supernovae [10].

The EII cross section is the sum of direct ionization (DI) channels and various autoionizing channels. An important autoionization channel is collisional excitation to a state which then autoionizes, a process commonly referred to as excitation-autoionization (EA). The most recent comprehensive review of EII theory and experiment is that of Dere [1] who covered all charge states of all elements from hydrogen through zinc. The vast majority of theoretical calculations for these systems have been performed using a distorted wave (DW) approach. Laboratory studies, though, have largely been limited to single pass experiments using ions beams contaminated by a typically unknown metastable fraction. Benchmark measurements exist only for those few isoelectronic sequences such as H-, Li-, and Na-like ions where one can generate pure ground state beams. Experimental work for all other sequences are usually compromised by unknown metastable fractions.

Linkemann *et al*. [11], Kenntner *et al*. [12], and more recently Hahn *et al*. [13–16] have carried out a sequence of EII measurements using the TSR heavy ion storage ring combined with a merged electron-ion beams arrangement. The storage ring geometry allows one to store the ions long enough for essentially all of the metastable levels to radiatively decay to their ground state. The resulting EII measurements provide unambiguous benchmark data for theory. The isoelectronic sequences studied to date include Li-like Si^{11+} and Cl^{14+} [12], Be-like S^{12+} [16], B-like Mg^{7+} [13], Na-like Fe^{15+} [11], Si-like Fe^{12+} [14], P-like Fe^{11+} [15], and S-like Fe^{10+} and Cl-like Fe^{9+} [Hahn *et al*. (in preparation)].

A comparison of the Fe^{11+} and Fe^{12+} results of Hahn *et al*. [14,15] with the recommended EII data of Dere [1] finds interesting discrepancies between theory and experiment. The measurements found that starting from the $3p$ EII threshold and extending up to the opening of the $2l$ EA channels (where l is the orbital angular momentum of the electron), theory falls below the experimental results for those systems which can undergo EA through excitation of a $3s$ electron. Hahn *et al*. [14,15] propose that this is due to the omission in the theoretical results of the $3s$ EA channel. They also found that theory lies above the experimental results at higher energies, when EA becomes possible via excitation of a $2l$ electron, and attribute this to an underestimate by theory of radiative stabilization versus autoionization for these higher energy autoionizating states.

In an attempt to help resolve the issues raised by Hahn *et al*. [14,15], we have carried out new calculations for EII of Fe^{11+} forming Fe^{12+}. Particularly close attention has been paid to the $3l$ EA channels near the EII threshold and to the $2l$ EA channels which opens up at higher energies. In Sec. II of this paper we describe the theoretical approach used. We present results and compare with previously published theoretical and experimental results in Sec. III. Lastly, a summary is given in Sec. IV.

II. THEORY

A. Method

Ionization of an atomic system can proceed either via a direct channel or via an indirect channel involving

autoionization of an intermediate system. The direct single ionization channel for an initial ion of charge state $q+$ results in a final ion of charge state $(q+1)+$. For any given atom A, DI for this single ionization process can be written as

$$e^- + A^{q+} \rightarrow A^{(q+1)+} + 2e^-. \quad (1)$$

Autoionization can proceed by way of a number of different channels. EA by ejection of a single electron involves

$$e^- + A^{q+} \rightarrow [A^{(q+)}]^{**} + e^- \rightarrow A^{(q+1)+} + 2e^-, \quad (2)$$

where the double star superscript signifies that the intermediate state is autoionizing. EA can also result in the emission of two or more electrons, a net multiple ionization event. Higher order autoionization processes involve dielectronic capture, which reduces the charge of the system and forms to a resonant state $[A^{(q-1)+}]^{**}$, followed by double autoionization, forming an $A^{(q+1)+}$ ion. This is known as resonant excitation double autoionization (REDA) if the two electrons are released sequentially and resonant excitation autodouble ionization (READI) if the two electrons are ejected simultaneously [11,17–19]. Neither of these channels are expected to contribute significantly to the total EII cross section for Fe^{11+}. The collisional excitation strengths for both the DI and EA channels are much greater than the dielectronic capture strengths for the REDA and READI channels. Hence we only consider DI and EA here.

We treat the direct and indirect ionization processes as independent. The total single ionization cross section is then given by

$$\sigma_{\rm tot} = \sum_f \sigma_f^{\rm DI} + \sum_j \sigma_j^{\rm CE} B_j^{\rm a}, \quad (3)$$

where $\sigma_f^{\rm DI}$ is the direct ionization cross section to the level f of $A^{(q+1)+}$, and $\sigma_j^{\rm CE}$ is the collisional excitation (CE) cross section in the A^{q+} ions to the level j which can then undergo autoionization by the emission of a single electron to form $A^{(q+1)+}$ with a branching ratio (BR) of $B_j^{\rm a}$. The BR for autoionization of level j by emission of a single electron can be expressed as

$$B_j^{\rm a} = \frac{\sum_k A_{jk}^{\rm a} B_k^{\rm r} + \sum_s A_{js}^{\rm r} B_s^{\rm a}}{\sum_k A_{jk}^{\rm a} + \sum_s A_{js}^{\rm r}}, \quad (4)$$

where $A_{jk}^{\rm a}$ is the autoionization rate from j to any level k of $A^{(q+1)+}$ and $A_{js}^{\rm r}$ is the radiative decay rate of A^{q+} from j to s. Some of the k levels may lie above the ionization limit for $A^{(q+1)+}$ and can further autotionize to form $A^{(q+2)+}$, resulting in a net double ionization event. The factor $B_k^{\rm r}$ accounts for the fraction of those k levels in $A^{(q+1)+}$ which radiatively relax instead, resulting in a net single ionization event. Similary, some of the s levels may still lie above the ionization limit for A^{q+} but can still radiatively relax to a bound state of A^{q+}, resulting in no net ionization. The term $B_s^{\rm a}$ accounts for the fraction of those s levels in A^{q+} which autoionize by the emission of a single electron, resulting in a net single ionization event. All of the branching ratios in Eq. (4) must be solved for recursively.

Cross sections were calculated using the flexible atomic code (FAC) [20] with a DW approximation. FAC uses a partial wave expansion for the continuum states. The expansion extends out to a maximum total orbital angular momentum $l_{\rm max}$. The value used for $l_{\rm max}$ for a given transition at a given collision energy was determined by increasing $l_{\rm max}$ until there was less than a 5% difference between the total cross section for $l_{\rm max}+1$ relative to the total cross section for $l_{\rm max}$. Values of up to $l_{\rm max}=36$ were used in the present calculations.

Data were generated at 20 different energies starting from near the EII threshold for DI and near the excitation threshold for CE. The calculations were carried out to about eight times the relevant threshold energy. The cross sections between energy grid points were interpolated with a standard cubic spline method. The potential used for the cross section is the post form of the scattering amplitude where all incident, scattered, bound, and ejected electrons see a V^{N-1} potential, where N is the total number of bound electrons in initial target ion [21,22]. One can also use the so-called prior form of the potential. In that case the incident and scattered electrons are calculated in a V^N potential but the bound and ejected electrons in a V^{N-1} potential [21,22]. We found no significant difference between these two approaches and used the post form for the results presented here.

B. Ionization channels considered

DI of a $3l$ electron for ground state Fe^{11+} can be expressed as

$$e^- + 2s^2 2p^6 3s^2 3p^3\ {}^4S_{3/2} \rightarrow 2s^2 2p^6 \left\{ \begin{array}{c} 3s^2 3p^2 \\ 3s 3p^3 \end{array} \right\} + 2e^-. \quad (5)$$

We do not include DI of a $2l$ electron because the resulting $2l$-hole system is predicted to autoionize 91% of the time to form Fe^{13+} [23], resulting in a net double ionization process.

The $3l$ EA channel opens up at the ionization threshold for the ground state. The first step in this EA process can be expressed

$$e^- + 2s^2 2p^6 3s^2 3p^3\ {}^4S_{3/2} \rightarrow 2s^2 2p^6 \left\{ \begin{array}{c} 3[s,p]^4 \\ 3[s,p]^3 3d \end{array} \right\} nl' + e^-, \quad (6)$$

where $3[s,p]^m$ indicates that m electrons are distributed between the s and p orbitals, $n \geqslant 4$, and we included only $l' \leqslant 5$. We consider both single electron excitation ($3l \rightarrow nl'$) and double electron excitation ($3[s,p]^2 \rightarrow 3lnl'$). Both excitations generate a system lying in the continuum of the initial ion. The system can then stabilize either to a bound system via autoionization (AI)

$$\mathrm{AI} \rightarrow 2s^2 2p^6 \left\{ \begin{array}{c} 3[s,p]^4 \\ 3[s,p]^3 3d \end{array} \right\} + 2e^-, \quad (7)$$

resulting in a net single ionization process, or it can relax via radiative decay (RD)

$$\mathrm{RD} \rightarrow 2s^2 2p^6 \left\{ \begin{array}{c} 3[s,p]^5 \\ 3[s,p]^4 3d \\ 3[s,p]^3 3d^2 \end{array} \right\} + h\nu + e^-, \quad (8)$$

leaving the charge state of the initial ion unchanged.

The $2l$ EA channel for excitation into the $n = 3$ shell begins as

$$e^- + 2s^2 2p^6 3s^2 3p^3\ {}^4S_{3/2} \rightarrow 2l^7 \left\{ \begin{array}{c} 3s^2 3p^4 \\ 3s^2 3p^3 3d \end{array} \right\} + e^-. \quad (9)$$

Net single ionization occurs when the system undergoes autoionization via

$$\mathrm{AI} \rightarrow 2l^8 \left\{ \begin{array}{c} 3[s,p]^4 \\ 3[s,p]^3 3d \end{array} \right\} + 2e^-. \quad (10)$$

The system can also stabilize by fluorescing

$$\mathrm{RD} \rightarrow 2l^8 \left\{ \begin{array}{c} 3[s,p]^5 \\ 3[s,p]^4 3d \end{array} \right\} + h\nu + e^-, \quad (11)$$

resulting in no net ionization.

The $2l$ EA channel via $2l \rightarrow nl'$ ($n \geqslant 4$) excitations begins with

$$e^- + 2s^2 2p^6 3s^2 3p^3\ {}^4S_{3/2} \rightarrow 2l^7 3s^2 3p^3 nl' + e^-, \quad (12)$$

where we considered only $l' \leqslant 5$. These excitation channels can undergo autoionization or radiative stabilibization via

$$\mathrm{AI} \rightarrow \left\{ \begin{array}{c} 2l^8 3[s,p]^4 \\ 2l^8 3[s,p]^3 nl' \\ 2l^7 3[s,p]^5 \end{array} \right\} + 2e^-, \quad (13)$$

$$\mathrm{RD} \rightarrow 2l^8 \left\{ \begin{array}{c} 3[s,p]^5 \\ 3[s,p]^4 nl' \end{array} \right\} + h\nu + e^-. \quad (14)$$

Additional care must be taken in the AI channels to account for the fact that the $2l^8 3[s,p]^3 nl'$ ($n \geqslant 6$) and $2l^7 3[s,p]^5$ levels lie above the ionization threshold of Fe^{12+} and can further autoionize to form Fe^{13+}. The AI and RD channels for the $2l^8 3[s,p]^3 nl'$ configurations are given by

$$\mathrm{AI} \rightarrow 2l^8 3[s,p]^3 + e^-, \quad (15)$$

$$\mathrm{RD} \rightarrow 2l^8 \left\{ \begin{array}{c} 3[s,p]^4 \\ 3[s,p]^3 3d \end{array} \right\} + h\nu, \quad (16)$$

and for the $2l^7 3[s,p]^5$ configurations by

$$\mathrm{AI} \rightarrow 2l^8 3[s,p]^3 + e^-, \quad (17)$$

$$\mathrm{RD} \rightarrow 2l^8 3[s,p]^4 + h\nu. \quad (18)$$

Clearly neither of these two AI channels contribute to the Fe^{11+} single ionization cross section.

III. RESULTS AND DISCUSSION

Various theoretical and experimental results for EII of ground state Fe^{11+} are shown in Fig. 1. The solid blue curve gives the FAC results of Dere [1]. Also plotted are the experimental results of Hahn *et al.* [15]. We have not included the earlier experimental results of Gregory *et al.* [24] as the unknown metastable fraction in their ion beam precludes an unambiguous comparison between theory and experiment.

Our total EII cross section is given by the solid red curve. The various components to this are plotted using colored dotted curves. The black one shows the $3l$ DI data. DI starts at $E_0 = 326.32$ eV, which is the calculated ionization energy of a $3p$ electron. This is in reasonable agreement with the ionization energy of 330.79 eV given by the NIST Atomic Spectra Database [25]. The $3l$ EA results for excitation to $4 \leqslant n \leqslant 35$ are plotted in blue. Our $2l \rightarrow 3l'$ EA calculations are given in green; and for EA via $2l \rightarrow nl'$ ($4 \leqslant n \leqslant 10$), the results are shown in red.

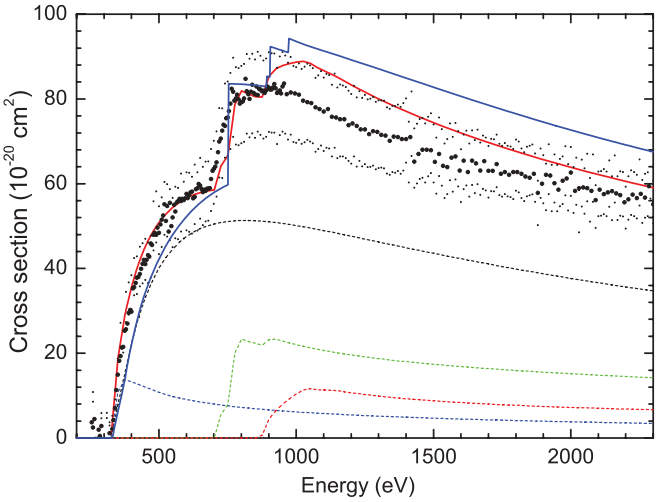

FIG. 1. (Color) EII cross section for ground state Fe^{11+} forming Fe^{12+}. Our total FAC results are shown by the solid red curve and the various components by the colored dotted curves: $3l$ DI in black, $3l \rightarrow nl'$ ($4 \leqslant n \leqslant 35$) EA in blue, $2l \rightarrow 3l'$ EA in green, and $2l \rightarrow nl'$ ($4 \leqslant n \leqslant 10$) in red. The earlier FAC results of Dere [1] are shown in blue. The experimental data of Hahn *et al.* [15] are plotted using the large filled circles and their 1σ experimental uncertainty is shown by the small filled circles.

From the EII threshold to about 700 eV, the theoretical results of Dere [1] and our $3l$ DI results both fall below the experimental results of Hahn *et al.* [15]. We find that the $3l$ EA channel can account for this difference. Below about 700 eV, our total cross section includes only these two channels. Excellent agreement between our results and the measurements can be seen in this energy range. It appears that Dere has left out many significant $3l$ EA channels from his results.

Our calculations indicate that about 85% of the $3l$ EA channel arises from dipole-forbidden transitions. Some of the strongest of these channels include excitations from $3s$ to ns ($n = 7$–12), $7d$, $7f$, and $8f$ as well as the $3s3p$ to $3d5f$ two-electron transition. For each of these channels, the peak cross section $\sigma_{\mathrm{max}}^{\mathrm{CE}}$ is over 1×10^{-21} cm^2 and B_j^{a} is greater than 0.99. Our calculated results include contributions from excitations to $4 \leqslant n \leqslant 35$. The peak $3l$ EA cross section from any individual higher n level is less than 0.5% of the peak in the total $3l \rightarrow nl'$ ($4 \leqslant n \leqslant 35$) EA cross section.

The $2l \rightarrow 3l'$ EA channel opens up at about 700 eV. The largest contributions to this EA channel are due to the $2p \rightarrow 3d$ dipole-allowed transition and the $2p \rightarrow 3p$ dipole-forbidden transition. For these channels, $\sigma_{\mathrm{max}}^{\mathrm{CE}}$ is greater than 5×10^{-21} cm^2 and B_j^{a} is greater than 0.95. For excitation of the $2s$ electron transition, $\sigma_{\mathrm{max}}^{\mathrm{CE}}$ is smaller than 5×10^{-21} cm^2 and B_j^{a} is greater than 0.97. About 35% of all $2l \rightarrow 3l'$ EA channels arises from dipole-forbidden transitions.

As can be seen in Fig. 1, the theoretical $2l \rightarrow 3l'$ EA channel appears to turn on about 20 eV higher in energy than the experimental data. We predict that this channel opens

up starting with the $2p \rightarrow 3p$ excitation at 703 eV. But experimental data turn on at about 680 eV. We attribute this difference to REDA and READI not being accounted for in our calculation. In the 680–700 eV energy range, each process can proceed via the dielectronic capture processes

$$e^- + 2s^2 2p^6 3s^2 3p^3\ {}^4S_{3/2} \rightarrow 2l^7 3l'^6 nl''. \quad (19)$$

REDA can occur for $n \geqslant 5$ via the sequential autoionization processes

$$2l^7 3l'^6 nl'' \rightarrow 2l^8 3l'^4 nl'' + e^- \rightarrow 2l^8 3l'^4 + 2e^-, \quad (20)$$

and READI can occur for $n \geqslant 3$ by simultaneous two electron emission through

$$2l^7 3l'^6 nl'' \rightarrow 2l^8 3l'^4 + 2e^-. \quad (21)$$

A detailed study of REDA and READI is beyond the scope of this paper and we have not pursued this issue further.

At about 860 eV the $2l \rightarrow nl'$ ($n \geqslant 4$) EA channels open up. Some of the strongest excitations include the $2p \rightarrow 4d$ and $5d$ dipole-allowed transitions as well as the dipole-forbidden $2p \rightarrow 4p$,$4d$, and $5p$, and $2s \rightarrow 4s$ transitions. All of these have values of $\sigma_{\max}^{\mathrm{CE}}$ greater than 1.0×10^{-21} cm^2. The autoionization BR is typically greater than 0.93 for these excitations. Dipole-forbidden transitions contribute about 35% to the total $2l \rightarrow nl'$ ($n = 4$–10) EA cross section, similar to the situation for $2l \rightarrow 3l'$ EA.

The contribution of the $2l \rightarrow nl'$ ($n > 4$) EA cross section decreases rapidly as n increases. This is due to autoionization of the intermediate $2l^7 3s^2 3p^3 nl'$ level to the $2l^8 3[s,p]^3 nl'$ ($n \geqslant 6$) and $2l^7 3[s,p]^5$ levels becoming more likely than radiative stabilization. These levels can then further autoionize resulting in a net double ionization event and a corresponding reduction in the single ionization cross section, as shown by the dotted curves in Fig. 2. By the time one reaches $n = 10$, the contribution of this EA channel to the single ionization cross section has become negligible.

According to our calculations, $2l \rightarrow nl'$ ($n \geqslant 4$) EA starts from the $2p \rightarrow 4s$ excitation at 859 eV with a clear, nearly steplike increase seen in the predicted cross section. However, no such corresponding increase is observed in the experimental results. Although the calculated total EII cross section does lie within the experimental uncertainty at these energies, that does not mean we find good agreement in this range. The experimental uncertainty represents primarily a uniform, multiplicative shift up or down to the data due to the ion current normalization. Were there a steplike increase in the measured cross section as large as that predicted by theory, then it would be clearly visible in the data. If there is a theoretical explanation for this difference, it is not obvious. We have verified the convergence of our calculations by increasing the partial wave expansion up to $l_{\max} = 50$ and find that the results do not change. We have also checked for the effects of configuration interaction (CI) between different $2l^7 3s^2 3p^3 nl'$ configurations for $n = 3$–10 using the same approach as we did for our CI studies of dielectronic recombination for Fe^{15+} [26]. However, we find that the CI does not change our results. We do note, though, that at these energies our results are in better agreement with the experimental data than the previous FAC calculation of Dere [1].

We have generated a Maxwellian rate coefficent $\alpha_1(T_e)$ for plasma modeling from our calculated EII cross section. Figure 3 shows the resulting rate coefficient compared the experimentally-derived rate coefficent of Hahn *et al.* [15] and the FAC results of Dere [1]. Also shown in the figure is the temperature range where Fe^{11+} is predicted to form in a

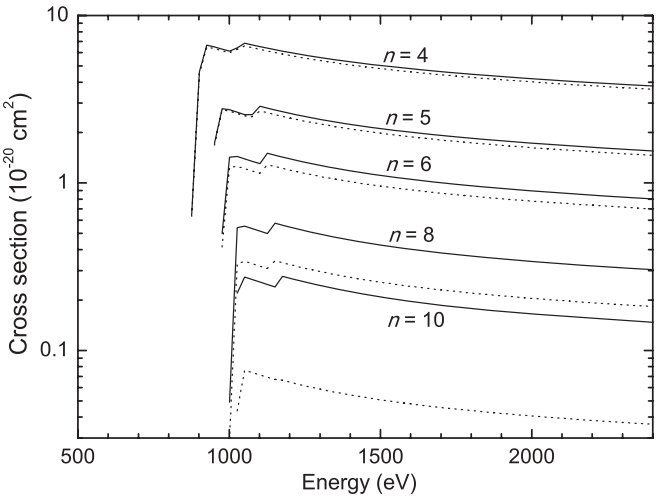

FIG. 2. EA cross section for ground state Fe^{11+} forming Fe^{12+} via $2l \rightarrow nl'$ excitations for labeled n levels. The solid curve shows the cross section setting $B_j^{\mathrm{a}} = 1.0$ which assume all excitations result in a net single ionization event. Taking into account that some of the excitations can result in a net double ionization event forming Fe^{13+}, the actual branching ratios can be significantly less than one, resulting in a much reduced cross section, as shown by the dotted curves. As a result, the net single ionization $2l \rightarrow nl$ EA cross section becomes insignificant for $n \geqslant 11$.

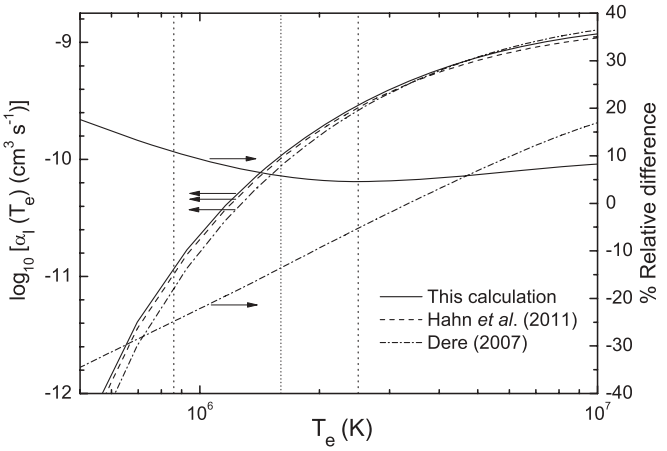

FIG. 3. EII rate coefficient for ground state Fe^{11+} forming Fe^{12+} derived from the present calculation. Also shown are the rate coefficients derived from the recent experiment of Hahn *et al.* [15] and from the previous FAC calculation by Dere [1]. Additionally displayed are the differences between these calculated rate coefficients and the experimental rate coefficient, divided by the experimental rate coefficient. Arrows are placed next to the curves to clarify the axis from which values are to be read off. The vertical dotted lines show the temperature range for collisional ionization equilibrium where the Fe^{11+} ion abundance is greater than 1% with the middle dotted line showing the temperature of maximum ion abundance [4].

TABLE I. Fifth-order polynomial fitting parameters used to reproduce the scaled ionization rate coefficient $\rho(x)$.

i	a_i
0	1.981190×10^{-5}
1	-6.820722×10^{-5}
2	2.714360×10^{-4}
3	-4.361066×10^{-4}
4	2.922002×10^{-4}
5	-6.392124×10^{-5}

[a]See Eqs. (22)–(24) in text.

collisionally ionized plasma [4]. In this range, our theoretical rate coefficient lies within 11% of the experimental results. This is to be contrasted with the results of Dere [1] which can differ from the experimental results by up to 25% over this range.

For convenience in plasma modeling we have fitted our calculated Maxwellian rate coefficient using the Burgess-Tully-type scaling [1] and a fifth-order polynomial. The temperature T_e was scaled as

$$x = 1 - \frac{\ln 2}{\ln(t+2)}, \tag{22}$$

where $t = \mathrm{k_B} T_e / E_0$. The rate coefficient α_I was scaled as

$$\rho = t^{1/2} E_0^{3/2} \alpha_\mathrm{I}(T_e) / E_1(1/t), \tag{23}$$

where E_1 is the first exponential integral. The scaled rate coefficient was fitted by the polynomial form

$$\rho = \sum_{i=0}^{5} a_i x^i. \tag{24}$$

The fit parameters are listed in Table I. The fit reproduces our calculated rate coefficient $\alpha_\mathrm{I}(T_e)$ to within 1.3% over the temperature range $T_e = (1 \times 10^5)$–(1×10^8) K.

IV. SUMMARY

We have calculated EII of P-like Fe^{11+} forming Si-like Fe^{12+} using FAC and a DW approximation. We focused our attention on the discrepancy between experiment and the previous FAC results. At the EII threshold, we find that inclusion of the $3l \rightarrow nl'$ EA channel can remove the discrepancy compared to the older FAC results. At higher energies, our more careful treatment of the $2l \rightarrow nl'$ ($n \geqslant 4$) EA reduces the discrepancy between experiment and theory, but does not remove it. At temperatures where Fe^{11+} forms in collisionally ionized plasmas, our FAC rate coefficient lies within 11% of the experimentally derived rate coefficient. This is an improvement over the up to 25% difference seen with the earlier FAC results.

ACKNOWLEDGMENTS

We thank M. Hahn for providing the experimental data and for using our data to generate Fig. 3. We also thank K. P. Dere and M. Hahn for many stimulating discussions. This work was supported by the Korean Ministry of Education, Science and Technology (MEST) and by grants from the NASA Astronomy and Physics Research and Analysis program and the NASA Solar Heliospheric Physics Supporting Research program.

[1] K. P. Dere, Astron. Astrophys. **466**, 771 (2007).
[2] T. R. Kallman and P. Palmeri, Rev. Mod. Phys. **79**, 79 (2007).
[3] N. J. Peacock, M. G. O'Mullane, R. Barnsley, and M. Tarbutt, Can. J. Phys. **86**, 277 (2008).
[4] P. Bryans, E. Landi, and D. W. Savin, Astrophys. J. **691**, 1540 (2009).
[5] D. Post, J. Abdallah, R. E. H. Clark, and N. Putvinskaya, Phys. Plasmas **2**, 2328 (1995).
[6] C. M. Brown *et al.*, Astrophys. J., Suppl. Ser. **176**, 511 (2008).
[7] C. R. Canizares *et al.*, Astrophys. J. Lett. **539**, L41 (2000).
[8] R. B. C. Henry, J. J. Cowan, and J. S. Sobeck, Astrophys. J. **709**, 715 (2010).
[9] J. R. Peterson, S. M. Kahn, F. B. S. Paerels, J. S. Kaastra, T. Tamura, J. A. M. Bleeker, C. Ferrigno, and J. G. Jernigan, Astrophys. J. **590**, 207 (2003).
[10] C. Badenes, E. Bravo, and J. P. Hughes, Astrophys. J. **680**, L33 (2008).
[11] J. Linkemann, A. Müller, J. Kenntner, D. Habs, D. Schwalm, A. Wolf, N. R. Badnell, and M. S. Pindzola, Phys. Rev. Lett. **74**, 4173 (1995).
[12] J. Kenntner *et al.*, Nucl. Instrum. Methods B **98**, 142 (1995).
[13] M. Hahn, D. Bernhardt, M. Lestinsky, A. Müller, O. Novotný, S. Schippers, A. Wolf, and D. W. Savin, Astrophys. J. **712**, 1166 (2010).
[14] M. Hahn *et al.*, Astrophys. J. **735**, 105 (2011).
[15] M. Hahn *et al.*, Astrophys. J. **729**, 76 (2011).
[16] M. Hahn *et al.*, Phys. Rev. A **85**, 042713 (2012).
[17] K. J. LaGattuta and Y. Hahn, Phys. Rev. A **24**, 2273 (1981).
[18] R. J. W. Henry and A. Z. Msezane, Phys. Rev. A **26**, 2545 (1982).
[19] N. R. Badnell and M. S. Pindzola, Phys. Rev. A **47**, 2937 (1993).
[20] M. F. Gu, Can. J. Phys. **86**, 675 (2008).
[21] S. M. Younger, Phys. Rev. A **26**, 3177 (1982).
[22] M. S. Pindzola, D. C. Griffin, and J. H. Macek, Phys. Rev. A **51**, 2186 (1995).
[23] J. S. Kaastra and R. Mewe, Astron. Astrophys. Suppl. Ser. **97**, 443 (1993).
[24] D. C. Gregory, L. J. Wang, F. W. Meyer, and K. Rinn, Phys. Rev. A **35**, 3256 (1987).
[25] Yu. Ralchenko, A. E. Kramida, J. Reader, and NIST ASD Team, NIST Atomic Spectra Database (ver. 4.1.0), http://physics.nist.gov/asd (2011).
[26] D.-H. Kwon and D. W. Savin, Phys. Rev. A **83**, 012701 (2011).